

# Efficient Calculation of Anharmonic Vibrational Spectra of Large Molecules with Localized Modes

Paweł T. Panek and Christoph R. Jacob\*<sup>[a]</sup>*In memory of Oliver Hampe*

The analysis and interpretation of the vibrational spectra of complex (bio)molecular systems, such as polypeptides and proteins, requires support from quantum-chemical calculations. Such calculations are currently restricted to the harmonic approximation. Here, we show how one of the main bottlenecks in such calculations, the evaluation of the potential energy surface, can be overcome by using localized modes instead of the commonly employed normal modes. We apply such local vibrational self-consistent field (L-VSCF) and vibrational configuration interaction (L-VCI) calculations to a cyclic water tetramer and a helical hexa-alanine peptide. The results show that the use of localized modes is equivalent to the commonly used

normal modes, but offers several advantages. First, a faster convergence with respect to the excitation level is observed in L-VCI calculations. Second, the localized modes provide a reduced representation of the couplings between modes that show a regular coupling pattern. This can be used to disregard a significant number of small two-mode potentials a priori. Several such reduced coupling approximations are explored, and we show that the number of single-point calculations required to evaluate the potential energy surface can be significantly reduced without introducing noticeable errors in the resulting vibrational spectra.

## 1. Introduction

Vibrational spectroscopy is a powerful technique that can be used to study the structure and dynamics of biomolecules in their natural environment.<sup>[1]</sup> It can probe fast processes that are inaccessible to X-ray diffraction or nuclear magnetic resonance (NMR) spectroscopy. Therefore, vibrational spectroscopy offers a unique experimental tool for investigating protein folding as well as unfolded or disordered proteins.<sup>[2,3]</sup> Besides conventional infrared (IR) and Raman spectroscopy, their chiral variants, vibrational circular dichroism (VCD)<sup>[4]</sup> and Raman optical activity (ROA),<sup>[5]</sup> have been shown to be suitable for the identification of residual structures in polyproline peptides<sup>[6,7]</sup> and  $\beta$ -sheet fibrils.<sup>[8]</sup> Additional insights can be obtained with multidimensional spectroscopic techniques, in particular two-dimensional (2D) IR spectroscopy.<sup>[9,10]</sup> Recently, 2D-IR spectroscopy has been used successfully to reconstruct the three-dimensional structure of protein complexes<sup>[11]</sup> and to observe the fast structural dynamics of proteins.<sup>[12,13]</sup>

However, because vibrational spectroscopy does not provide direct structural information, these achievements largely rely on theoretical work complementing the experiments. Usually, the well-known harmonic approximation<sup>[14]</sup> is the first choice for the calculation of vibrational spectra.<sup>[1]</sup> Modern computational methods are pushing the limit of the system sizes that can be treated in such calculations with first-principles quan-

tum-chemical methods. For instance, full quantum-chemical calculations of the ROA spectra of large polypeptide models<sup>[15–17]</sup> and even of full proteins<sup>[18]</sup> have become possible in the past years. By focusing on only specific normal modes<sup>[19,20]</sup> or on those with a significant intensity,<sup>[21,22]</sup> additional computational gains are possible without introducing approximations. Moreover, by applying additional approximations,<sup>[23]</sup> harmonic vibrational spectra of large biomolecular systems can be made even more efficient, albeit at the price of possibly introducing significant errors.<sup>[24,25]</sup>

However, the harmonic approximation often does not reproduce experimental vibrational spectra accurately. This becomes particularly relevant for flexible biological molecules, which include strongly anharmonic floppy vibrations. Pronounced anharmonic effects are also present in modes involved in hydrogen bonds or noncovalent interactions.<sup>[26,27]</sup> Gas-phase experiments can be used to reveal such anharmonic effects for biological model systems,<sup>[28–31]</sup> because they allow for a direct comparison of accurate experimental data with quantum-chemical calculations. Anharmonicities are especially relevant for the calculation of vibrational spectra of polypeptides and proteins, and it can be expected that anharmonicities might significantly alter the intensity patterns in the VCD and ROA spectra of such biomolecular systems. Moreover, the harmonic approximation allows only for fundamental transitions, whereas it has been shown that overtone and combination bands are often needed to reproduce experimental spectra accurately.<sup>[32]</sup> These overtones and combination bands are probed directly in 2D-IR experiments, which makes using computational

[a] P. T. Panek, Dr. C. R. Jacob  
Karlsruhe Institute of Technology (KIT)  
Center for Functional Nanostructures and Institute of Physical Chemistry  
Wolfgang-Gaede-Str. 1a, 76131 Karlsruhe (Germany)  
E-mail: christoph.jacob@kit.edu  
Homepage: <http://www.christophjacob.eu>

methods beyond the harmonic approximation mandatory for investigating 2D spectra.

Numerous computational first-principle methods have been developed to tackle vibrational anharmonicities. Time-dependent methods are based on classical molecular dynamics simulations, from which vibrational spectra can be extracted as the Fourier transformation of autocorrelation functions (see, for example, Thomas et al.<sup>[33]</sup>). However, even though these methods employ a fully anharmonic potential energy surface, the quantum-mechanical anharmonic effects are not included in such approaches because of the classical treatment of the nuclear dynamics. In fact, for low temperatures, only the harmonic vibrational frequencies are recovered and the anharmonic shifts for combination bands and overtones are not reproduced.<sup>[33, 34]</sup>

In contrast, time-independent methods aim to provide a direct solution of the nuclear Schrödinger equation. Here, two main approaches are well-established: vibrational perturbation theory (VPT) and variational methods. The first approach assumes that the anharmonicities are a perturbation of the harmonic normal modes and uses analytical expressions depending on third, fourth, and possibly higher derivatives of the potential energy surface at the equilibrium geometry.<sup>[32]</sup> In this case, the treatment of resonances is problematic and requires special attention.<sup>[35–37]</sup> Note that such resonances become more abundant for larger molecules, for which almost degenerate harmonic vibrational frequencies are very common. The latter approach is based on the variational solution of the nuclear Schrödinger equation with methods that are conceptually similar to those used in electronic structure theory. The most important examples of such methods are the vibrational self-consistent field (VSCF) and vibrational configuration interaction (VCI) methods.<sup>[38]</sup>

For both variational and perturbative approaches, the main computational bottleneck that limits their applicability to small and medium-sized molecules, respectively, is the evaluation of the potential energy surface. This either requires calculation of the higher-order energy derivatives or calculation of the potential energy surface on an integration grid. The number of such higher-order derivatives or the number of grid points grows rapidly—at least quadratically—with the size of the molecules, which presently precludes anharmonic vibrational calculations for larger molecules. Here, this main bottleneck is addressed by developing variational methods (i.e. VSCF and VCI) based on localized vibrational modes instead of the commonly used normal modes. We show that a localization of the normal modes leads to a representation of the potential energy surface that is sparse for large molecules and that allows many couplings between vibrational modes to be omitted without compromising the overall accuracy.

## 2. Expansion of the Potential Energy Surface

For the calculation of vibrational spectra, one has to solve the nuclear Schrödinger equation given by Equation (1):

$$\hat{H}(\mathbf{R}) \Psi_n^{\text{nuc}}(\mathbf{R}) = E_n \Psi_n^{\text{nuc}}(\mathbf{R}) \quad (1)$$

with the nuclear wavefunction  $\Psi_n^{\text{nuc}}$  for state  $n$  and with the nuclear Hamiltonian in atomic units given in Equation (2):

$$\hat{H}(\mathbf{R}) = - \sum_{l=1}^{N_{\text{nuc}}} \frac{1}{2m_l} \sum_{\alpha=x,y,z} \frac{\partial^2}{\partial R_{l\alpha}^2} + V(\mathbf{R}) \quad (2)$$

where  $m_l$  is the mass of the  $l$ -th nucleus,  $R_{l\alpha}$  are the Cartesian coordinates of the nuclei, the vector  $\mathbf{R} = \{R_{l\alpha}\}$  collects all Cartesian nuclear coordinates, and  $V(\mathbf{R})$  is the potential energy surface defined by the solution of the clamped-nuclei electronic Schrödinger equation for nuclear positions  $\mathbf{R}$ . For simplicity, displacement coordinates can be introduced, that is, the origin is chosen such that for the equilibrium geometry  $\mathbf{R}_0 = 0$ . By introducing mass-weighted coordinates  $R_{l\alpha}^{(m)} = \sqrt{m_l} R_{l\alpha}$ , the nuclear Hamiltonian simplifies to Equation (3):

$$\hat{H} = - \frac{1}{2} \sum_{l=1}^{N_{\text{nuc}}} \sum_{\alpha=x,y,z} \frac{\partial^2}{(\partial R_{l\alpha}^{(m)})^2} + V(\mathbf{R}^{(m)}) \quad (3)$$

In the harmonic approximation, the potential energy surface is approximated by a second-order Taylor expansion at the equilibrium structure, given by Equation (4):

$$V(\mathbf{R}^{(m)}) \approx V(0) + \frac{1}{2} \sum_{l,j=1}^{N_{\text{nuc}}} \sum_{\alpha,\beta=x,y,z} H_{l\alpha,j\beta}^{(m)} R_{l\alpha}^{(m)} R_{j\beta}^{(m)} \quad (4)$$

with the potential energy of the equilibrium structure  $V(0)$  and the mass-weighted Hessian given by Equation (5):

$$H_{l\alpha,j\beta}^{(m)} = \frac{1}{\sqrt{m_l m_j}} \left( \frac{\partial^2 E}{\partial R_{l\alpha} \partial R_{j\beta}} \right)_0 \quad (5)$$

where the subscript 0 indicates that the second derivatives are taken at the equilibrium geometry. This Hessian is diagonalized by a unitary matrix  $\mathbf{Q}$  as given in Equation (6):

$$\mathbf{H}^{(q)} = \mathbf{Q}^T \mathbf{H}^{(m)} \mathbf{Q} \quad (6)$$

which contains the normal modes  $\mathbf{Q}^j$  as its columns. The diagonal Hessian  $\mathbf{H}^{(q)}$  contains squared angular frequencies of the vibrations  $H_{ii}^{(q)} = \omega_i^2 = 4\pi^2 \nu_i^2$ , where  $\nu_i$  is the vibrational frequency of the  $i$ -th normal mode. The normal modes define the normal coordinates, as Equation (7):

$$q_i = \sum_{l=1}^{N_{\text{nuc}}} \sum_{\alpha=x,y,z} Q_{l\alpha}^i R_{l\alpha}^{(m)} = \sum_{l=1}^{N_{\text{nuc}}} \sum_{\alpha=x,y,z} \sqrt{m_l} Q_{l\alpha}^i R_{l\alpha} \quad (7)$$

In these normal coordinates, the nuclear Schrödinger equation in the harmonic approximation is given by Equation (8):

$$\left( - \frac{1}{2} \sum_{i=1}^M \frac{\partial^2}{\partial q_i^2} + \frac{1}{2} \sum_{i=1}^M H_{ii}^{(q)} q_i^2 \right) \Psi_n^{\text{harm}}(\mathbf{q}) = E_n \Psi_n^{\text{harm}}(\mathbf{q}) \quad (8)$$

where  $M$  is the number of normal modes and the vector  $\mathbf{q} = \{q_j\}$  collects all normal coordinates. In the harmonic approximation, the normal coordinates are decoupled and the exact nuclear wavefunctions are given by Equation (9):

$$\Psi_n^{\text{harm}}(\mathbf{q}) = \Psi_n^{\text{harm}}(\mathbf{q}) = \prod_{i=1}^M \phi_i^{n_i}(q_i) \quad (9)$$

where  $\phi_i^{n_i}(q_i)$  is a harmonic oscillator wavefunction for the  $i$ -th normal mode (i.e. with vibrational frequency  $\nu_i$ ) in its  $n_i$ -th state. Here, a collective index  $\mathbf{n} = \{n_i\}$ , containing the vibrational quantum numbers for each mode, is introduced to label the nuclear wavefunctions. The six (five for linear molecules) normal modes describing translations and rotations can be separated from the remaining vibrational modes because in the harmonic approximation all modes are decoupled; that is, only  $M = 3N_{\text{nuc}} - 6$  normal modes are considered.

The full anharmonic nuclear Hamiltonian can be now be rewritten in the normal coordinates as Equation (10):

$$\hat{H} = -\frac{1}{2} \sum_{i=1}^M \frac{\partial^2}{\partial q_i^2} + V(\mathbf{q}) \quad (10)$$

If all  $3N_{\text{nuc}}$  normal modes are included, this nuclear Hamiltonian is still exact. However, one usually separates translations and rotations from the  $M = 3N_{\text{nuc}} - 6$  vibrational modes. For the anharmonic nuclear Hamiltonian, this separation can be achieved by using the Eckart conditions, resulting in the Watson Hamiltonian.<sup>[39]</sup> This contains an additional term describing the rotational–vibrational coupling, which has been neglected in Equation (10). It has been shown that, for small molecules, the error arising from this approximation can be up to 10–20  $\text{cm}^{-1}$ . However, because the Coriolis coupling coefficients are inversely proportional to the moment of inertia, for large systems the error can be expected to be significantly smaller.<sup>[40]</sup>

It is noteworthy that the nuclear Hamiltonian can also be defined in more general coordinates. One can use more natural curvilinear coordinates to solve the vibrational problem.<sup>[41–43]</sup> However, for those coordinates, the form of the kinetic energy operator is more sophisticated, which further complicates the solution of the nuclear Schrödinger equation. The present study is restricted to the use of rectilinear coordinates within the simplified Hamiltonian of Equation (10).

## 2.1. N-Mode Expansion in Normal Modes

The main computational difficulty at this point is posed by the need to evaluate the potential energy surface  $V(\mathbf{q})$ . A complete evaluation of  $V(\mathbf{q})$  is feasible only for the smallest systems because of the many degrees of freedom. Therefore, to calculate vibrational properties of larger molecules, an approximated potential energy surface has to be introduced. To this end, a hierarchical expansion of the potential energy surface is employed in Equation (11):<sup>[44,45]</sup>

$$V(\mathbf{q}) = \sum_i^M V_i^{(1)}(q_i) + \sum_{i<j}^M V_{ij}^{(2)}(q_i, q_j) + \dots \quad (11)$$

Here, the potential energy surface is decomposed into contributions coming from a limited number of normal modes. The one-mode and two-mode terms are defined as, Equations (12) and (13):

$$V_i^{(1)}(q_i) = V_i^0(q_i) - V(0) \quad (12)$$

$$V_{ij}^{(2)}(q_i, q_j) = V_{ij}^0(q_i, q_j) - \sum_{r \in \{i,j\}} V_r^{(1)}(q_r) - V(0) \quad (13)$$

where  $V_i^0(q_i)$  and  $V_{ij}^0(q_i, q_j)$  denote the potential energy for structures distorted along the normal coordinate  $q_i$  or the two normal coordinates  $q_i$  and  $q_j$ , respectively, and all other coordinates are kept at their equilibrium positions. Higher-order (three-mode, four-mode, etc.) contributions can be defined analogously. By truncating this  $n$ -mode expansion, the dimensionality of the potential energy surface can be limited. However, the description of the surface can be systematically improved by including higher-order terms in the expansion. It has been reported that at least the three-mode terms should be included for small molecules to achieve an accuracy of ca. 1  $\text{cm}^{-1}$ .<sup>[46,47]</sup> However, the inclusion of all three-mode potentials becomes infeasible for all but the smallest molecules. Therefore, only the one-mode and two-mode contributions are considered here.

In the harmonic approximation the normal modes are fully decoupled, thus only the one-mode potentials are nonzero, and are given by Equation (14):

$$V_i^{(1)}(q_i) = \frac{1}{2} q_i^2 H_i^{(q)} \quad (14)$$

The terms of the  $n$ -mode expansion can be evaluated on a grid. For the one-mode potentials, one commonly uses equally-spaced grids of  $N_{\text{grid}}$  points along normal coordinates (i.e. a set of normal coordinates), given in Equation (15):

$$q_i^{(k)} = -q_i^{\text{max}} + (k - 1) \Delta q \quad \text{with } k = 1, \dots, N_{\text{grid}} \quad (15)$$

with the grid spacing  $\Delta q = 2q_i^{\text{max}} / (N_{\text{grid}} - 1)$  and the grid range defined by Equation (16):

$$q_i^{\text{max}} = \sqrt{\frac{2(A + \frac{1}{2})}{\omega_i}} \quad (16)$$

where  $A$  is the maximal (harmonic) vibrational quantum number that is considered, and where  $\omega_i$  is the (harmonic) angular frequency of the  $i$ -th normal mode. Thus, the maximal grid value  $q_i^{\text{max}}$  is the distance along the normal coordinate for which the total energy of the  $A$ -th harmonic vibrational state is equal to the harmonic potential energy. For the two-mode po-

tentials, the grid is a product of the linear grids of the considered modes, which results in a square grid of  $N_{\text{grid}}^2$  points. The number of grid points must be sufficient to describe the potential and wavefunction accurately, while at the same time the amplitude, and thus the  $A$  parameter of Equation (16), has to be large enough to cover a sufficient range of the normal coordinate. The number of required single-point calculations grows rapidly with the system size because for the anharmonic potentials every grid point requires a single-point quantum-chemical calculation. If only one- and two-mode potentials are included, the number of required single-point calculations is  $M \cdot N_{\text{grid}} + \frac{M \cdot (M-1)}{2} N_{\text{grid}}^2$ , and the computational effort for each single-point calculation also grows at least linearly with the system size. This makes vibrational anharmonic calculations very computationally demanding already for medium-sized molecules, and unfeasible for large systems such as polypeptides and proteins.

To address this bottleneck, several methods have been developed to limit the number of two-mode potentials that have to be evaluated. Pele and Gerber suggested that not all of the normal modes are strongly coupled and that, therefore, some couplings can be neglected.<sup>[48]</sup> The strongest coupling was assumed to occur for modes presenting similar displacements of the same groups of atoms, and the authors proposed a statistical tool to measure this similarity. Benoit proposed a prescreening scheme based on semiempirical methods, which can be used to decide which two-mode potentials can be neglected.<sup>[49]</sup> In both schemes, couplings below a given threshold can be neglected without losing good overall accuracy of the vibrational calculation. Similar prescreening approaches have been explored for VPT calculations.<sup>[50]</sup>

However, the number of non-negligible couplings grows with the system size. Furthermore, in many cases, all modes are strongly coupled and none or a very small number of couplings could be neglected. As an example, a hexa-alanine peptide in a  $3_{10}$ -helical conformation is considered. The molecular structure of this model system is shown in Figure 1. Specific-

ly, the amide I and amide II bands are studied, which are characteristic bands in the vibrational spectrum of polypeptides. The first, lying at around  $1650 \text{ cm}^{-1}$ , is mainly a C=O stretching motion, whereas the latter, lying at around  $1550 \text{ cm}^{-1}$ , is a combination of the N–H in-plane bending and C–N stretching vibrations. In Figure 2a the couplings of the normal modes belonging to amide I and amide II bands of hexa-alanine are shown. The magnitude of these couplings are measured as sums of absolute values of the two-mode potentials on all grid points for each pair of modes,<sup>[49]</sup> and is given by Equation (17):

$$\eta_{ij} = \sum_k \sum_l \left| V_{ij}^{(2)}(q_i^{(k)}, q_j^{(l)}) \right| \quad (17)$$

where a grid with 16 points was used.

For the amide I band, a strong coupling is observed for nearly all pairs of normal modes. Only for three pairs (1st↔6th, 3rd↔6th, and 4th↔6th) the couplings are significantly smaller and could, most likely, be neglected; however, this would not significantly reduce the total number of two-mode potentials that have to be evaluated. The amide II modes are generally weaker coupled, but also in this case only a few of the couplings can be neglected. This even distribution of the coupling strengths over all pairs arises from the fact that the normal modes are delocalized over several residues of the peptide, which is shown for one of the amide I normal modes in Figure 1a. This leads to a strong coupling between all of the pairs of modes. Therefore, in the space of such delocalized normal modes, most of the couplings are important, and none of the prescreening methods can bring significant computational savings.

## 2.2. Expansion in Localized Modes

To overcome the large number of strong non-negligible couplings arising from the delocalization of the normal modes in large molecules, a different approach is presented here. Instead of expanding the potential energy surface in terms of normal modes, the expansion can be performed in rigorously defined localized modes. Such localized modes can be obtained by performing a unitary transformation of the normal modes<sup>[51]</sup> and have previously been established as a tool for analyzing (harmonic) vibrational spectra of large molecules.<sup>[15, 16, 52–54]</sup> A detailed description for the methodology for localizing vibrational normal modes was presented previously,<sup>[51]</sup> and we will, therefore, only provide a brief overview.

Here, we proceed as follows: First the normal modes are obtained by diagonalizing the molecular Hessian [see Eq. (6)]. A subset of  $k$  normal modes, for example those modes corresponding to one band in the spectrum, is chosen and collected in a matrix  $\mathbf{Q}^{\text{sub}}$ . To these modes a unitary transformation  $\mathbf{U}$  is applied [Eq. (18)]:

$$\tilde{\mathbf{Q}}^{\text{sub}} = \mathbf{Q}^{\text{sub}} \mathbf{U} \quad (18)$$

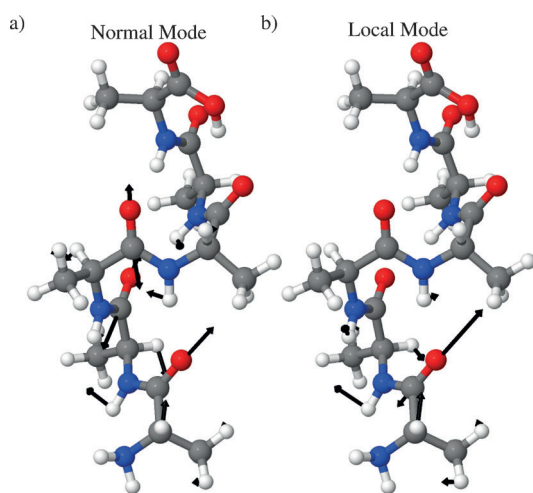


**Figure 1.** The optimized molecular structure of the helical hexa-alanine peptide used as a test case. a) One of the amide I normal modes ( $1666.96 \text{ cm}^{-1}$ ). b) A corresponding localized mode for the amide I band ( $1667.20 \text{ cm}^{-1}$ ).

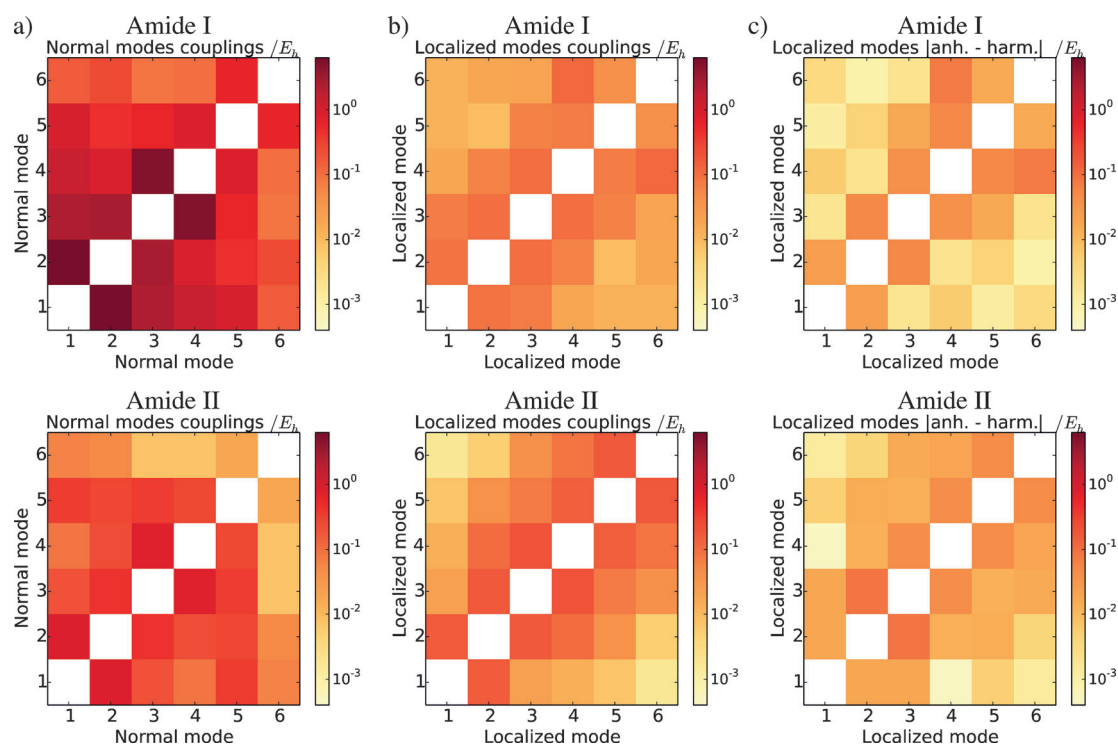


**Figure 2.** Magnitude  $\eta_{ij}$  of the coupling between pairs of amide I (top) and amide II (bottom) modes in hexa-alanine with respect to different coordinates. The magnitude of the couplings is measured according to Equation (17) and plotted here on a logarithmic scale. a) The magnitudes of the two-mode couplings with respect to normal mode coordinates, and b) with respect to localized mode coordinates. c) Magnitude of the anharmonic part of the two-mode couplings with respect to localized modes, obtained from the difference between the anharmonic and harmonic couplings.

Here and in the following, the tilde denotes quantities referring to the localized modes. The unitary transformation is determined such that it maximizes a function  $\xi(\tilde{\mathbf{Q}}^{\text{sub}})$  measuring the localization of the subset of the modes (see Ref. [51]). The localization then yields a set of localized modes, each of which is usually localized on a different residue. As an example, one of the localized modes obtained for the amide I band in hexa-alanine is shown in Figure 1 b).

Once the localized modes are obtained it is noteworthy that these modes are no longer the eigenvectors of the mass-weighted Hessian  $\mathbf{H}^{(m)}$ . Instead, the Hessian with respect to the localized modes is given by Equation (19):

$$\tilde{\mathbf{H}}^{\text{sub}} = \mathbf{U}^T \mathbf{H}^{(q),\text{sub}} \mathbf{U} \quad (19)$$

The diagonal elements of the  $\tilde{\mathbf{H}}^{\text{sub}}$  deliver fictitious vibrational frequencies  $\tilde{\nu}_i$  of the localized modes [Eq. (20)]:

$$\tilde{H}_{ii}^{\text{sub}} = \tilde{\omega}_i^2 = 4\pi^2 \tilde{\nu}_i^2 \quad (20)$$

and the off-diagonal elements  $\tilde{H}_{ij}^{\text{sub}}$  describe the harmonic coupling between pairs of localized modes. Note that the nuclear Hamiltonian of Equation (10) is invariant under unitary transformation. Therefore, it is possible to employ localized mode coordinates [Eq. (21)]:

$$\tilde{q}_i = \sum_{l=1}^{N_{\text{nuc}}} \sum_{a=x,y,z} \tilde{Q}_{la}^i R_{la}^{(m)} \quad (21)$$

instead of the normal mode coordinates. However, the  $n$ -mode expansion is not invariant with respect to a transformation of the coordinates. In particular, within the harmonic approximation, the one-mode potentials are now determined by the diagonal elements of  $\tilde{\mathbf{H}}^{\text{sub}}$  as Equation (22):

$$V_i^{(1)}(\tilde{q}_i) = \frac{1}{2} \tilde{q}_i^2 \tilde{H}_{ii}^{\text{sub}} \quad (22)$$

while the two-mode potentials no longer vanish in the harmonic approximation, but are now given by Equation (23):

$$V_{ij}^{(2)}(\tilde{q}_i, \tilde{q}_j) = \tilde{q}_i \tilde{q}_j \tilde{H}_{ij}^{\text{sub}} \quad (23)$$

thus, they are determined by the off-diagonal elements of  $\tilde{\mathbf{H}}^{\text{sub}}$ .

In Figure 2b the magnitude of the two-mode potentials with respect to localized modes is shown for the amide I and amide II bands of hexa-alanine. Here, the localization has been performed for each of these bands separately. In both cases, the localized modes are more weakly coupled than the normal modes, and the strongest coupling can be observed to the first and second nearest neighbors. This sparsity of couplings with respect to localized modes comes from the fact that each of the localized modes is localized on a single residue, so that

different atoms are involved in each of the localized vibrations. This reduces the size of all couplings significantly. Especially for the amide I band, all but the first-nearest neighbor couplings appear to be negligible. The remaining anharmonic couplings are slightly larger for the amide II band than for the amide I band. Taken together, Figure 2 suggests that significant computational savings might be achieved by performing anharmonic vibrational calculations in the basis of localized modes instead of normal modes, because the reduction in the number of couplings could allow many couplings to be neglected a priori.

The use of local vibrational modes has previously been shown to be advantageous for treating anharmonicities in computational vibrational spectroscopy in various contexts. Most prominent are vibrational exciton models<sup>[55–58]</sup> in which local anharmonic oscillators are coupled harmonically. Such models are extensively used in combination with molecular dynamics simulations to describe 2D-IR spectra.<sup>[57–59]</sup> The parameters entering vibrational exciton models (i.e. the local mode frequencies and their couplings as well as the anharmonicity of the local modes) are usually obtained empirically by fitting to experimental data or quantum-chemical calculations of model compounds, or by assuming more simplified models, such as the transition dipole coupling model.<sup>[60,61]</sup> In particular for the amide I band in polypeptides and proteins (see, for example Refs. [62],[63] and references therein) and for the O–H stretch vibrations in water (see, for example Ref. [64] and references therein), such parameters are well-established.

Nevertheless, local modes have so far not found widespread use in first-principles anharmonic calculations. Rauhut employed localized modes to study size-consistency effects in VCI calculations.<sup>[65]</sup> Bowman and co-workers introduced a local-monomer (LMon) model<sup>[66]</sup> to study the anharmonic vibrational spectra of water clusters, which was later also extended to clusters of HCl.<sup>[67]</sup> In this model, local modes from (embedded) monomer calculations are employed to perform VSCF/VCI calculations in the space of the monomer local modes. The resulting frequencies can then be modified by using a Hückel-like correction.<sup>[68]</sup> The use of optimized coordinates that minimize the VSCF energy has also been explored.<sup>[69]</sup> Often, such optimized coordinates turn out to be more localized than the normal mode coordinates. Recently, it was shown that such optimized coordinates lead to a faster convergences with respect to the excitation level in VCI<sup>[70]</sup> and vibrational coupled cluster (VCC) calculations.<sup>[71]</sup> However, all these methods either introduce *ad hoc* assumptions or do not lead to computational saving in the evaluation of the potential energy surface.

### 3. VSCF and VCI in Localized Modes

To explore the potential advantages of localized modes for anharmonic vibrational calculations, we have implemented VSCF and VCI methods in terms of rigorously defined localized modes. These methods will be termed L-VSCF and L-VCI, respectively. As there are several comprehensive descriptions of VSCF and VCI available,<sup>[38,47,72]</sup> we will only recall the most im-

portant steps here and focus on the specific details of our implementation.

In L-VSCF, a product ansatz is used for the vibrational wavefunction [Eq. (24)]:

$$\Psi_n(\tilde{\mathbf{q}}) \approx \psi_n(\tilde{q}_1, \dots, \tilde{q}_M) = \prod_i^M \phi_i^{n_i}(\tilde{q}_i) \quad (24)$$

Here,  $\phi_i^{n_i}(\tilde{q}_i)$  is a so-called modal for the  $i$ -th localized mode, and  $n_i$  is the vibrational quantum number for this modal. Every modal is further expanded as a linear combination of distributed Gaussians (DGs) basis functions.<sup>[73]</sup> Each of these basis functions is centered on a single point of the modal's grid, where the same grid, of  $N_{\text{grid}}$  points, as used for the evaluation of the potential is applied [Eq. (25)]:

$$\phi_i^{n_i}(\tilde{q}_i) = \sum_m^{N_{\text{grid}}} c_m^{n_i} \chi_m(\tilde{q}_i) \quad (25)$$

with  $c_m^{n_i}$  being the expansion coefficients and [Eq. (26)]:

$$\chi_m(\tilde{q}_i) = \left(\frac{2A_m}{\pi}\right)^{1/4} e^{-A_m(\tilde{q}_i - \tilde{q}_i^{(m)})^2} \quad (26)$$

where  $\tilde{q}_i^{(m)}$  is the center of the DG function, and  $A_m$  is a grid-spacing-dependent parameter, which for an equally-spaced grid is given by Equation (27):

$$A_m = \frac{C^2}{\Delta q^2} \quad (27)$$

with  $C$  being a free parameter, here taken as  $C=0.7$ . Such a choice of the basis set and the grid allows for the efficient evaluation of the required integrals with Gauss–Hermite quadrature. For details, we refer to Ref. [73]. Inserting this wavefunction ansatz into the nuclear Schrödinger equation [Eq. (1)] and applying the variational principle reduces the many-body problem to a set of one-mode equations for each modal [Eq. (28)]:

$$\hat{h}_i^n(\tilde{q}_i) |\phi_i^{n_i}(\tilde{q}_i)\rangle = \varepsilon_i^n |\phi_i^{n_i}(\tilde{q}_i)\rangle \quad (28)$$

with the effective Hamiltonian [Eq. (29)]:

$$\hat{h}_i^n(\tilde{q}_i) = -\frac{1}{2} \frac{\partial^2}{\partial \tilde{q}_i^2} + V_i^{(1)}(\tilde{q}_i) + V_i^n(\tilde{q}_i) \quad (29)$$

containing an effective mean-field potential [Eq. (30)]:

$$V_i^n(\tilde{q}_i) = \sum_{j \neq i}^M \left\langle \phi_j^{n_j}(\tilde{q}_j) \left| V_{ij}^{(2)}(\tilde{q}_i, \tilde{q}_j) \right| \phi_j^{n_j}(\tilde{q}_j) \right\rangle \quad (30)$$

The one-mode equations reduce to a matrix eigenvalue problem, which can be solved to obtain the modal energies  $\varepsilon_i^n$  and, indirectly, the expansion coefficients  $c_m^{n_i}$  as eigenvalues

and eigenvectors, respectively. In our implementation, the eigenvalue problem is solved by means of the collocation method.<sup>[74]</sup> Note that for a given effective potential, this method not only provides the modal for the considered state, denoted by the vector  $\mathbf{n}$ , but also gives solutions for all values of the vibrational quantum number  $n_i$  (up to  $N_{\text{grid}}$ ). The effective potential implicitly depends on the wavefunction and, therefore, the set of one-mode equations must be solved in a self-consistent manner.

Due to the mean-field potential, VSCF calculations do not include the correlation between the modals. By analogy to electronic structure calculations, several methods to tackle the lack of correlation have been developed. Among others, a perturbative MP2-like correction (CC-VSCF), the vibrational configuration interaction method (VCI), or the vibrational coupled cluster method (VCC) are available. For comprehensive reviews of the available methods, see Refs. [38], [75], and [76].

The vibrational configuration interaction (VCI) method proposed by Bowman et al.<sup>[77]</sup> becomes useful when the coupling (correlation) of the molecular motions is strong and can no longer be treated as a perturbation and/or if degeneracies in the vibrational energies occur. In this method, a total (VCI) wavefunction for a considered vibrational state is built as a linear combination of  $N_{\text{states}}$  VCI basis states [Eq. (31)]:

$$\Psi_i(\mathbf{q}) \approx \Psi_i^{\text{VCI}}(\mathbf{q}) = \sum_i^{N_{\text{states}}} c_i^{(i)} \psi_{\mathbf{n}_i}^0(\mathbf{q}) \quad (31)$$

Here, the functions  $\psi_{\mathbf{n}_i}^0$  (with the collective index  $\mathbf{n}_i = \{n_i^j\}$ ) are constructed from the VSCF modals  $\phi_i^{n_i^j,0}$  obtained for vibrational quantum number  $n_i^j$  with the effective potential constructed from the ground-state modals (i.e. for  $\mathbf{n}=0$ ). This is indicated by the additional superscript 0. Note that using modals obtained for different VSCF states is also common,<sup>[78]</sup> but will not be considered here. Applying the variational principle with the ansatz of Equation (31) leads to a CI eigenvalue equation with the CI-matrix [Eq. (32)]:

$$\begin{aligned} \langle \psi_{\mathbf{n}_i}^0 | \hat{H} | \psi_{\mathbf{n}_j}^0 \rangle &= \sum_i^M \left\langle \phi_i^{n_i^j,0} \left| -\frac{1}{2} \frac{\partial^2}{\partial \mathbf{q}_i^2} + V_i^{(1)} \right| \phi_i^{n_i^j,0} \right\rangle \prod_{j \neq i}^M \delta_{n_i^j n_j^j} \\ &+ \sum_{i < j}^M \left\langle \phi_i^{n_i^j,0} \phi_j^{n_j^j,0} \left| V_{ij}^{(2)} \right| \phi_i^{n_i^j,0} \phi_j^{n_j^j,0} \right\rangle \prod_{k \neq i,j}^M \delta_{n_i^k n_k^k} \end{aligned} \quad (32)$$

The diagonalization of this CI-matrix yields VCI energies and VCI wavefunction coefficients. In practice, the CI expansion in Equation (31) is limited to a given order of excitation. For example, one can consider VCI singles (VCIS) with a ground state and singly excited states. Further inclusion of doubly excited configurations results in VCISD, and the additional consideration of triple excitations is denoted as VCISDT. It has been shown that inclusion of even higher excitations—at least quadruples in VCISDTQ—is required for an accuracy of  $1 \text{ cm}^{-1}$  in small molecules. However, the inclusion of higher excitation levels also increases the computational effort to construct and diagonalize the CI-matrix,<sup>[65,79]</sup> because the size of the VCI

matrix grows factorially with both the number of modes and the excitation level. Thus, eventually the construction and diagonalization of the VCI matrix will become the bottleneck for large molecules. Neff and Rauhut reviewed and proposed several methods to improve the efficiency of different steps of VCI calculations for large systems.<sup>[78]</sup> At the same time, the need to include higher excited states also increases the computational effort for the evaluation of the potential energy surface. The wavefunctions of higher excited states extend over a wider range of space compared with the ground state, and thus requires the use of a larger number of grid points.

Once the VCI eigenvalues and eigenvectors are obtained, the infrared intensities for the considered transitions can be calculated. The IR intensity of the transition between two VCI states, namely  $i$  and  $j$ , is proportional to the square of the transition dipole moment [Eq. (33)]:

$$I_{i \rightarrow j} \propto \left| \langle \Psi_i^{\text{VCI}} | \boldsymbol{\mu}(\mathbf{q}) | \Psi_j^{\text{VCI}} \rangle \right|^2 \quad (33)$$

This transition dipole moment can be evaluated as Equation (34):

$$\langle \Psi_i^{\text{VCI}} | \boldsymbol{\mu}(\mathbf{q}) | \Psi_j^{\text{VCI}} \rangle = \sum_{I,J} c_i^{(I)} c_j^{(J)} \left\langle \prod_p^M \phi_p^{n_p^I,0} \left| \boldsymbol{\mu}(\mathbf{q}) \right| \prod_q^M \phi_q^{n_q^J,0} \right\rangle \quad (34)$$

With the dipole moment surface expanded in the same way (and on the same grids) as the potential energy surface (i.e. in the  $n$ -mode expansion), Equation (35) is obtained:

$$\boldsymbol{\mu}(\mathbf{q}) = \sum_i^M \boldsymbol{\mu}_i^{(1)}(q_i) + \sum_{i < j}^M \boldsymbol{\mu}_{ij}^{(2)}(q_i, q_j) + \dots \quad (35)$$

where the one-mode and two-mode contributions are defined in analogy to Equations (12) and (13), the integrals of Equation (34) transform into corresponding one- and two-mode integrals, which can be evaluated numerically with Gauss–Hermite quadrature.

#### 4. Test Case: Water Tetramer

As an initial test case, a water tetramer was considered. This example is a well-established test case for anharmonic vibrational calculations<sup>[68,80,81]</sup> and an analytical potential energy surface is available.<sup>[82]</sup> The considered tetramer has a symmetric equilibrium structure, which is depicted in Figure 3. Its calculated harmonic vibrational spectrum shows three characteristic bands, each consisting of four normal modes. One is assigned to the water bending vibration and appears at ca.  $1675 \text{ cm}^{-1}$ . At ca.  $3600$  and at ca.  $3910 \text{ cm}^{-1}$  two bands are observed that are due to the O–H stretching vibrations. The band at lower wavenumber can be assigned to the stretching vibrations of the O–H groups that form the intermolecular hydrogen bonds (Bond-OH), whereas the latter is assigned to the stretching of the O–H groups not participating in hydrogen bonds (Free-OH). For noninteracting water molecules, the respective four

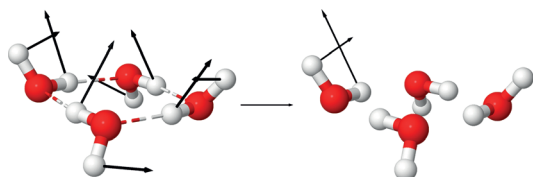


**Figure 3.** Molecular structure of the considered symmetric water tetramer, together with one of the bending normal modes (left) and a corresponding localized mode (right).

modes of each molecule would have the same vibrational frequencies. For each of the three bands, the interaction splits this 4-fold degeneracy into one lowest state, a doubly degenerate middle state, and one highest state.

As a first test, VSCF and L-VSCF calculations were performed separately for these three characteristic bands using the harmonic potential energy surface. For the L-VSCF, the localization was performed for each of these three bands separately. The corresponding one- and two-mode potentials were calculated at each grid point according to Equation (14) for the case of normal modes, and Equations (22) and (23) for localized modes (see Section 2.2). The use of the harmonic potential energy surface provides a quick check of the implementation and the integration grid. In particular, VSCF and L-VSCF calculations should reproduce the harmonic or localized mode frequencies, respectively. In addition, the L-VCI calculations should reproduce the normal mode harmonic frequencies.

Here, the close connection of L-VCI with a harmonic potential energy surface to the (harmonic) vibrational exciton model<sup>[55,83]</sup> (for a concise review, see for example Ref. [84]) becomes clear: In the harmonic case, the VSCF effective potential vanishes, with respect to both normal and localized modes. Thus, the resulting modals, from which the VCI basis states are constructed, are harmonic oscillator wavefunctions corresponding to the normal or localized mode angular frequencies  $\omega_i$  and  $\tilde{\omega}_i$ , respectively. With respect to localized modes, the singly-excited manifold of the VCI matrix then contains the diagonal elements  $H_{ij}^{Cl(1)} = 3\tilde{\omega}_i/2 + \sum_i \tilde{\omega}_i/2$  and the off-diagonal elements  $H_{ij}^{Cl(1)} = \tilde{H}_{ij}^{sub}/(2\sqrt{\tilde{\omega}_i\tilde{\omega}_j})$ . After subtracting the energy expectation value of the L-VSCF ground state  $H^{Cl(0)} = \sum_i \tilde{\omega}_i/2$  from the diagonal elements, these reduce to  $H_{ij}^{Cl(1)} = \tilde{\omega}_i$ . Thus, the L-VCI matrix in the singly-excited manifold is exactly equal to the Hamiltonian used in harmonic vibrational exciton models. If we assume that the off-diagonal elements are much smaller than the diagonal elements (i.e.  $H_{ij}^{Cl(1)} \ll H_{ii}^{Cl(1)}$ ), and that the differences between local mode frequencies  $|\tilde{\omega}_i - \tilde{\omega}_j|$  are small compared with the frequencies themselves, the L-VCI matrix in the singly-excited manifold becomes equal to the coupling matrix introduced in Ref. [51]. This coupling matrix has the harmonic vibrational frequencies as its eigenvalues, which should thus be recovered in L-VCI calculations. The differences arising from the assumptions made above are corrected by the inclusion of higher excited states in the L-VCI, but should be negligible for the examples considered here.

The results obtained for the water tetramer with a harmonic potential energy surface are presented in Table 1. The VSCF

**Table 1.** Vibrational frequencies obtained for the characteristic bands of a water tetramer obtained with VSCF, L-VSCF, and L-VCI for a harmonic potential energy surface. Here, harm. denotes the normal modes harmonic frequencies obtained from the diagonalization of the Hessian and used to construct the potential energy surface, and  $\tilde{\nu}$  denotes localized modes harmonic frequencies. All values given in  $\text{cm}^{-1}$ .

Normal modes harm.	Localized modes						
	VSCF	$\tilde{\nu}$	L-VSCF	L-VCI S	SD	SDT	SDTQ
<b>Bend mode</b>							
1669	1669	1681	1681	1669	1669	1669	1669
1676	1676	1681	1681	1676	1676	1676	1676
1676	1676	1681	1681	1676	1676	1676	1676
1701	1702	1681	1681	1702	1702	1701	1701
<b>Bond-OH stretch mode</b>							
3575	3575	3600	3600	3575	3575	3575	3575
3600	3600	3600	3600	3600	3600	3600	3600
3600	3600	3600	3600	3600	3600	3600	3600
3625	3625	3600	3600	3625	3625	3625	3625
<b>Free-OH stretch mode</b>							
3900	3900	3909	3909	3900	3900	3900	3900
3909	3909	3909	3909	3909	3909	3909	3909
3909	3909	3909	3909	3909	3909	3909	3909
3918	3918	3909	3909	3918	3918	3918	3918

calculations reproduce the harmonic frequencies obtained from the diagonalization of the Hessian, and a proper splitting of the degeneracy is observed. The localized mode frequencies show a 4-fold degeneracy because each of them corresponds to a similar vibration localized on a different water molecule, as shown in Figure 3. As expected, L-VSCF reproduces the frequencies of the localized modes and maintains this degeneracy. Already L-VCI, where only single excitations are included, reproduces the harmonic frequencies of the normal modes and the correct degeneracy pattern. Inclusion of higher excitations, namely doubles, triples, and quadruples, does not change the frequencies.

Calculations were then performed with the full anharmonic potentials—obtained with the WHBB water potential.<sup>[82]</sup> In this case, VSCF and VCI calculations were carried out in terms of both normal and local modes. For each band, the calculations were performed in the space limited to the considered band, hence only two-mode potentials between modes belonging to this band were included, and all the other two-mode potentials were neglected. The calculated vibrational frequencies are given in Table 2. A VSCF ground-state wavefunction was used as starting point for performing the VCI calculations.

For the bending modes, VSCF leads to a lowering of the harmonic frequencies. Subsequently, the VCI frequencies converge quickly when increasing the excitation level. With respect to localized modes, L-VSCF delivers a 4-fold degeneracy, which is split already for L-VCI. Subsequently, the L-VCI frequencies do not change with the inclusion of higher excitations. For the bending modes, L-VCI already reproduces the VCI SDTQ frequencies of the normal mode with a maximal deviation of  $1 \text{ cm}^{-1}$ .

The role of the anharmonicities becomes more important in the case of the Bond-OH stretch mode. Here, the normal modes VSCF does not reproduce the proper degeneracy pat-

**Table 2.** Vibrational frequencies obtained for the characteristic bands of a water tetramer obtained with VSCF, L-VSCF, and L-VCI for the fully anharmonic potential energy surface. All values given in  $\text{cm}^{-1}$ .

Normal modes					Localized modes				
VSCF	VCI				L-VSCF	L-VCI			
S	SD	SDT	SDTQ	S	SD	SDT	SDTQ		
Bend mode									
1655	1656	1655	1655	1654	1667	1655	1655	1655	1655
1663	1664	1663	1663	1662	1667	1662	1662	1662	1662
1663	1664	1663	1663	1662	1667	1662	1662	1662	1662
1692	1692	1691	1691	1690	1667	1690	1690	1690	1690
Bond-OH stretch mode									
3454	3508	3438	3479	3407	3421	3398	3398	3398	3398
3454	3575	3470	3510	3422	3421	3422	3422	3422	3422
3508	3576	3470	3510	3422	3421	3422	3422	3422	3422
3549	3601	3492	3534	3448	3421	3440	3440	3440	3440
Free-OH stretch mode									
3849	3874	3798	3835	3761	3770	3758	3758	3758	3758
3795	3893	3806	3842	3766	3770	3770	3770	3770	3770
3796	3899	3806	3843	3767	3770	3770	3770	3770	3770
3875	3900	3812	3849	3786	3770	3781	3781	3781	3781

tern. This degeneracy pattern is, however, recovered with VCI methods, already for VCIS, but the convergence with respect to the excitation level is very slow. When going from VCISDT to VCISDTQ, changes in the vibrational frequencies of up to  $88 \text{ cm}^{-1}$  are still found. As previously, L-VSCF delivers degenerate frequencies, but these are already split for L-VCIS. The frequencies do not change upon inclusion of higher excitations, and they are very close to normal mode VCISDTQ frequencies, with maximal deviation of  $9 \text{ cm}^{-1}$ . However, it appears that, in contrast to L-VCI, VCISDTQ in normal modes is not yet converged with respect to the excitation level, and that the deviations can be attributed to errors in the VCISDTQ results.

Similarly, for the Free-OH stretch modes, the VSCF in normal modes results in an incorrect degeneracy pattern. The proper degeneracy is reproduced with VCI methods if at least double excitations are included. The frequencies converge slowly up to VCISDTQ. In the localized modes, an initial 4-fold L-VSCF degeneracy is transformed into a proper picture already for L-VCIS, and as for the other bands, the frequencies do not change with the inclusion of higher excitations. For this band, deviations between VCISDTQ and L-VCISDTQ frequencies are observed for each mode, and reach at most  $5 \text{ cm}^{-1}$ . Again, the oscillating convergence behavior of the VCI calculations employing normal modes suggests that even VCISDTQ may not yet be converged with respect to the excitation level.

These initial tests showed that the choice of the number of grid points used here is sufficient for the harmonic potential energy surface used in the calculations. Both VSCF and L-VSCF reproduced the harmonic vibrational frequencies of normal and localized modes, respectively. As expected, L-VCI with the harmonic potentials, already with only single excitation included, recovers the corresponding harmonic frequencies of the normal modes. For the anharmonic

potential energy surfaces, VCI and L-VCI converged to the same vibrational frequencies, with a maximal deviation of  $9 \text{ cm}^{-1}$ . However, L-VCI converged significantly faster, and it appears that the inclusion of only single excitations is sufficient. In contrast, VCI required inclusion of higher excitations and, in some cases, does not seem to be converged even for VCISDTQ, which accounts for the differences between VCI in normal modes and L-VCI.

## 5. Limiting the Number of Anharmonic Couplings: Hexaalanine as a Test Case

As a more complex test case, hexa-alanine was investigated. Here, two characteristic bands, namely amide I and amide II, are considered. With the full anharmonic potential energy surfaces, VSCF and VCI calculations in terms of both normal and localized modes were performed. Similar to the water tetramer test case, the anharmonic potentials were calculated only in terms of the investigated modes. Hence, the VSCF and VCI calculations were performed in limited spaces, neglecting coupling to modes not belonging to the considered bands. The calculated vibrational frequencies are presented in Table 3. First, the VSCF and L-VSCF calculations were performed, and the resulting ground-state wavefunctions were used as starting point for the VCI and L-VCI calculations, respectively.

For the amide I band, the normal mode VCI vibrational frequencies converge slowly up to VCISDTQ, so that it is unclear whether the results are already converged at this excitation level. In the localized modes space, the L-VSCF frequencies differ from the VSCF in terms of normal modes, with maximal deviation of  $8 \text{ cm}^{-1}$ . However, L-VCIS already yields frequencies that are converged with respect to the excitation level, and which are within maximally  $3 \text{ cm}^{-1}$  compared with VCISDTQ.

In the case of the amide II band, VSCF and VCI frequencies are very similar, with a maximal deviation of  $1 \text{ cm}^{-1}$ , and VCIS

**Table 3.** Vibrational frequencies obtained for the amide I and amide II bands of hexa-alanine obtained with VSCF, L-VSCF, and L-VCI for the fully anharmonic potential energy surface. All values given in  $\text{cm}^{-1}$ .

Normal modes					Localized modes				
VSCF	VCI				L-VSCF	L-VCI			
S	SD	SDT	SDTQ	S	SD	SDT	SDTQ		
Amide I									
1649	1654	1648	1650	1645	1648	1644	1644	1644	1644
1656	1655	1649	1652	1647	1648	1650	1650	1650	1650
1662	1667	1662	1664	1660	1657	1657	1657	1657	1657
1669	1672	1669	1671	1668	1663	1665	1665	1665	1665
1673	1673	1673	1675	1672	1672	1672	1672	1672	1672
1739	1739	1739	1741	1739	1739	1739	1739	1739	1739
Amide II									
1470	1469	1469	1469	1469	1475	1470	1470	1470	1470
1482	1482	1482	1482	1482	1481	1482	1482	1481	1481
1494	1494	1494	1494	1494	1500	1493	1494	1493	1493
1511	1511	1511	1511	1511	1505	1510	1511	1510	1510
1514	1514	1514	1514	1514	1510	1514	1514	1514	1514
1614	1614	1614	1614	1614	1614	1614	1614	1614	1614

already delivers converged results. Similar to the amide I band, the L-VCIS already reproduces normal mode VCI results, with maximal discrepancies of  $1\text{ cm}^{-1}$ . Again, in this case, the inclusion of higher excitations does not change the L-VCI frequencies. The results show that for both the amide I and the amide II bands, L-VCIS provides accurate and converged results.

As already discussed in Section 2.2, the localized modes are strongly coupled to at most the second nearest neighbor (see Figure 2), and the coupling patterns are very regular and systematic. In contrast, because of the delocalization in the normal modes space, the couplings are irregular and do not provide any prospect of neglecting a significant number of two-mode potentials. The potential advantage of the localized modes for neglecting small couplings was our motivation to use them in anharmonic vibrational calculations. The analysis of the coupling patterns led us to the assumption that the evaluation of the two-mode potentials could be limited only to those pairs of localized modes that are relatively strongly coupled. Nevertheless, the gain in terms of the computational time should not compromise the overall accuracy of the vibrational spectra, with respect to both the frequencies and the intensities. To explore such L-VCI calculations with a reduced number of anharmonic couplings, different approximations have been tested. The results for both vibrational frequencies and infrared intensities are presented in Table 4, and the spectra are plotted in Figure 4.

The L-VCIS results obtained for the full anharmonic potentials were chosen as our reference because they already provide converged frequencies and intensities. These can be compared to the different approximated models, both in terms of the normal and localized modes. The different approximated models can be characterized by the number of single-point calculations required to obtain the anharmonic potentials and dipole-moment surfaces. All the potentials were evaluated on 16-

point grids. Thus, if no couplings are neglected, in total 3936 single-point calculations are required for each band, 96 for the one-mode potentials, and 3840 for the two-mode potentials.

First, in terms of the normal modes, the potential energy surface and the dipole moment surface can be approximated quadratically and linearly, respectively, leading to the double-harmonic approximation—denoted here as “Harmonic” in Table 4 and Figure 4. The double-harmonic approximation for both the amide I and amide II bands yields spectra that are

**Table 4.** Vibrational frequencies ( $\nu$ ) and infrared intensities ( $I$ ) for the amide I and amide II bands in hexa-alanine obtained with the different reduced coupling approximations introduced in the main text. Frequencies and intensities are given in  $\text{cm}^{-1}$  and  $\text{km mol}^{-1}$ , respectively.

Normal modes harmonic		anharmonic VSCF-d		Localized modes									
$\nu$	$I$	$\nu$	$I$	L-VCIS		L-VCIS-1		-12		-1+h		-0+h	
				$\nu$	$I$	$\nu$	$I$	$\nu$	$I$	$\nu$	$I$	$\nu$	$I$
<b>Amide I</b>													
1652	110	1660	110	1644	120	1645	135	1644	113	1644	111	1644	110
1658	643	1654	636	1650	653	1651	411	1650	626	1650	650	1650	642
1667	118	1672	117	1657	104	1656	137	1657	121	1658	107	1658	106
1674	359	1669	356	1665	347	1665	451	1665	320	1665	344	1665	354
1682	221	1673	216	1672	210	1672	273	1672	239	1672	214	1672	211
1753	327	1739	319	1739	323	1739	339	1739	332	1739	318	1738	317
<b>Amide II</b>													
1465	154	1467	155	1470	160	1471	183	1469	166	1470	161	1471	163
1476	101	1478	102	1482	112	1482	161	1482	125	1482	114	1481	116
1486	67	1488	67	1494	61	1494	68	1494	61	1494	62	1494	57
1502	196	1507	197	1511	208	1508	255	1510	197	1511	209	1510	205
1505	264	1512	265	1514	254	1515	128	1514	247	1514	251	1514	256
1616	51	1614	52	1614	53	1614	53	1614	53	1614	53	1614	53

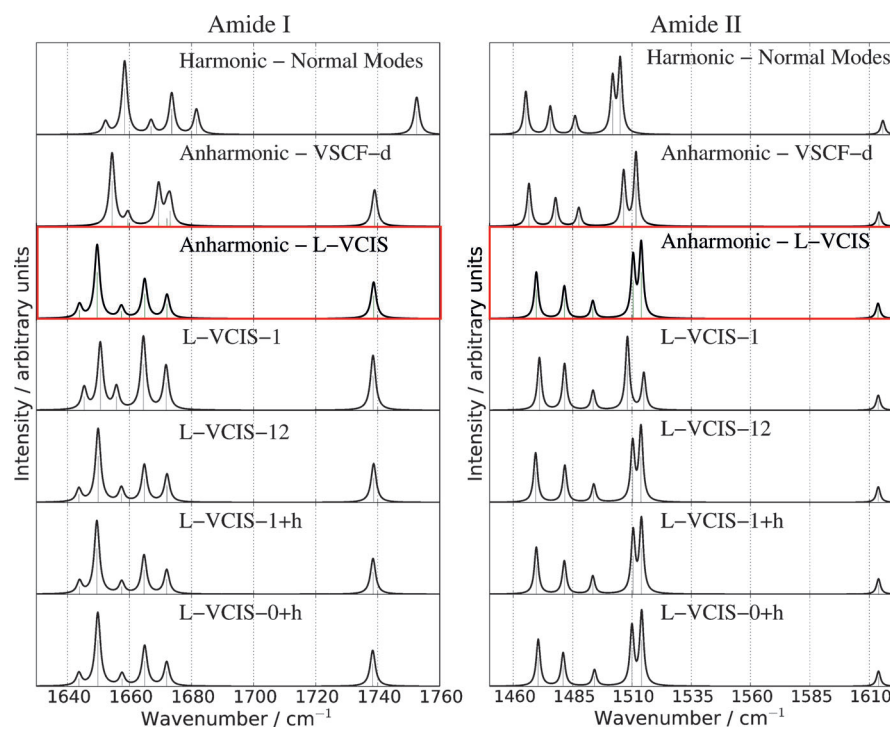


**Figure 4.** Infrared spectra for the amide I and amide II bands in hexa-alanine obtained with the different reduced coupling approximations introduced in the main text. The red frame marks the reference spectra obtained with L-VCIS and fully anharmonic one- and two-mode potentials.

shifted by maximally 14 and 9  $\text{cm}^{-1}$  with respect to the fully anharmonic L-VCIS reference, respectively. The intensity pattern is well reproduced, with some minor deviations of maximally 14 and 12  $\text{kmol}^{-1}$ , respectively. The harmonic approximation can be defined as neglecting the (anharmonic) one-mode and all two-mode potentials, thus no single-point calculations are required to obtain the anharmonic potentials. As for the investigated amide I and amide II bands, there is no reasonable way of neglecting only some of the couplings (compare Figure 2a). Therefore, all the anharmonic two-mode potentials and two-mode dipole moments were neglected, and only one-mode properties were included, introducing so-called diagonal VSCF, which is denoted as VSCF-d in Table 4 and Figure 4. The VSCF-d calculations require only 96 single-point calculations to obtain the one-mode potentials and dipole moments. In this case, the spectrum lies closer to the reference, with a maximal deviation of 12  $\text{cm}^{-1}$  for the amide I band and 6  $\text{cm}^{-1}$  for the amide II band. However, the discrepancies in the shape of the spectra, especially for the amide I band, are clearly visible in Figure 4.

Due to regular patterns observed for the couplings in terms of the localized modes, a few possible reduced models were tested. Initially, only the first nearest neighbor anharmonic couplings and two-mode dipole moment contributions were considered, and all other contributions were neglected. This model is denoted as L-VCIS-1, and requires 1376 single-point calculations to obtain the potential energy surface. The resulting spectrum shows that, for both of the bands, the frequencies are slightly shifted and the intensities pattern is incorrect. The intensities deviate from the reference by up to 242  $\text{kmol}^{-1}$  for the amide I and 126  $\text{kmol}^{-1}$  for the amide II band.

The second nearest neighbor anharmonic contributions were then also included, which gives the L-VCIS-12 model. This improves the spectra significantly. The frequencies of the reference are reproduced, with maximally 1  $\text{cm}^{-1}$  discrepancy, and the deviation of intensities is notably smaller. However, the inclusion of the second nearest neighbor couplings increases the total number of single-point calculations to 2400.

From the (nondiagonal) Hessian with respect to localized modes,  $\tilde{\mathbf{H}}^{\text{sub}}$ , the harmonic two-mode potentials in terms of the localized modes can be evaluated without requiring additional single-point calculations. These harmonic two-mode potentials were added to the L-VCIS-1 model in the place of the omitted anharmonic potentials; thus, the first nearest neighbor couplings remained anharmonic, whereas the remaining couplings were replaced by harmonic two-mode potentials. This model is denoted as L-VCIS-1+h. Now, the spectra are very similar to the references. The frequencies are very well reproduced, and only minor deviations of at most 9  $\text{kmol}^{-1}$  for the amide I can be observed for the intensities. However, the total computational cost is the same as for the L-VCIS-1 model, namely 1376 single points, because the harmonic couplings are obtained as a result of the localization procedure.

Finally, in the most approximate reduced coupling model L-VCIS-0+h, all of the anharmonic two-mode potentials were substituted with their harmonic analogues. Here, for the dipole

moment surface only one-mode contributions were taken into account. The computational cost of this model decreases significantly, because it requires only 96 single-point calculations to generate the anharmonic one-mode potentials. Note that such an approximation is similar to the one underlying vibrational exciton models, in which anharmonic local oscillators are coupled harmonically. The spectra present very good agreement with the references, and there are only minor discrepancies of the intensities, lying in the region of 11  $\text{kmol}^{-1}$ . Nevertheless, the overall agreement is better than for the case with L-VCIS-1, where at least the first nearest neighbor anharmonic couplings were included. At the same computational cost, calculations in the normal modes space (VSCF-d) yield spectra closer to those obtained within the double harmonic approximation, with worse reproduction of the intensities with respect to the L-VCIS reference.

The tests carried out show that the use of the localized modes can decrease the computational cost of anharmonic vibrational calculations significantly. These modes present regular coupling patterns, which can be used for an a priori reduction of the number of two-mode potentials in the anharmonic calculations. In our ultimate approximation, LVCIS-0+h, the anharmonic two-mode potentials can be easily substituted by the harmonic potentials obtained from the localization procedure, without losing much accuracy. In contrast, the delocalized and mutually strongly coupled normal modes do not allow for such an efficient prescreening.

## 6. Conclusions

We explored the use of localized modes for anharmonic vibrational calculations. To this end, we employed the previously developed methodology for the localization of normal modes<sup>[51]</sup> and used the resulting localized modes obtained for specific bands for VSCF and VCI calculations. This gave rise to the L-VSCF and L-VCI methods, which we applied to a symmetric water tetramer and a hexa-alanine peptide as test cases.

Our tests demonstrate that L-VSCF/L-VCI reproduces the results obtained with conventional VSCF/VCI calculations in terms of normal modes. However, it turns out that L-VCI provides a significantly faster convergence with respect to the excitation level than conventional VCI and, for the examples considered here, L-VCIS provides converged results. This feature can lead to a reduction of the computational cost for both the L-VCI calculation itself and for the construction of the potential energy surface, because fewer grid points are required for the smaller excitation space.

Furthermore, the localized modes are each localized on a particular residue of the peptide or on a single molecule of the cluster. Therefore, they are less coupled than the delocalized normal modes. The magnitudes of the couplings follow a regular pattern, and the strongest couplings occur with the nearest neighbors, whereas other couplings are negligible. This low number of couplings between modes, which is not present for normal modes, helps to address the main bottleneck of the anharmonic vibrational calculations, which is the tedious evaluation of the anharmonic two-mode potentials. Thus, sev-

eral reduced coupling models were presented, in which some of the anharmonic two-mode potentials were omitted. This made it possible to reduce the total number of single-point calculations and to decrease the scaling of the number of required single-point calculations with the system size. We showed that the omitted anharmonic two-mode potentials can be substituted with their harmonic equivalents, which were provided by the localization of the modes. In our ultimate approximation, all of the anharmonic two-mode potentials were substituted with their harmonic equivalents. The presented results show that this approximation provides vibrational spectra that are in very good agreement with the fully anharmonic reference.

In the present study, we applied L-VSCF and L-VCI only to specific spectroscopically relevant spectral bands such as the amide I or amide II bands of polypeptides. The localization and the subsequent anharmonic calculations were performed in a space limited to the modes included in the considered bands, whereas couplings between the considered band and other vibrational modes were completely neglected. However, such couplings can be included in future calculations. Here, the locality can be exploited further by considering two-mode potentials only for localized modes that are, for example, localized on the same residue. To this end, we will explore reliable screening criteria for discarding couplings between localized modes a priori in our future work.

We note that although only VSCF and VCI were considered here, the use of localized modes is not restricted to these methods. In particular, VPT could also be formulated in terms of localized modes, which might make it possible to restrict the number of higher-order derivatives that have to be evaluated. Similarly, the use of localized modes is not restricted to the inclusion of only two-mode potentials, but could also be used to restrict the number of three-mode potentials (and possibly higher-order contributions) that have to be evaluated to those combinations of localized modes that are strongly coupled.

## Computational Methodology

To study the properties of the water tetramer discussed herein, the analytical water potential WHBB, developed by Bowman and co-workers,<sup>[82]</sup> was employed. By using this potential, the equilibrium structure was optimized with the PyADF<sup>[85]</sup> and SciPy<sup>[86]</sup> packages. For hexa-alanine, geometry optimizations as well as single-point, dipole moment, and gradient calculations were carried out by using density-functional theory with the Turbomole 6.5 program package.<sup>[87,88]</sup> The BP86 exchange-correlation functional<sup>[89,90]</sup> with Ahlrichs' def-TZVP basis sets<sup>[91]</sup> in combination with the resolution of identity (RI) approximation and suitable auxiliary basis set was used.<sup>[92,93]</sup> For both of the systems, using the same methods, semi-numerical Hessians, normal modes, and harmonic frequencies were obtained by using the SNF module<sup>[94]</sup> of MoViPac.<sup>[95]</sup> The normal modes were localized by using the LocVib tools.<sup>[51,95]</sup>

L-VSCF and L-VCI have been implemented in a newly developed Python code "Vibrations", which makes use of the PyADF scripting framework<sup>[85]</sup> and the NumPy<sup>[96]</sup> and SciPy<sup>[86]</sup> packages. After reading in normal or localized modes, Vibrations generates the respec-

tive grids. In this study, the choice of the number of grid points and of the amplitude parameters was tested extensively. These tests showed that for both of the studied systems, the amplitude parameter describing the range of the grid [parameter *A* of Eq. (16)] should be greater than or equal to 14, and this value was used throughout this study. The grids for the water tetramer were built of 20 points for each considered mode, whereas those for hexa-alanine employed 16 points. Subsequently, Vibrations uses PyADF to obtain the one-mode and two-mode potentials as well as—if necessary—dipole moment surfaces. Here, these have been calculated with the methods mentioned above, namely the WHBB potential for the water tetramer and BP86/TZVP for hexa-alanine. The VSCF and L-VSCF calculations were performed, and the resulting ground-state wavefunctions were then used in VCI and L-VCI calculations, respectively. It has to be emphasized that, in this study, all (L)-VSCF and (L)-VCI calculations were performed in limited spaces; thus, only couplings between the considered modes were included. As a result, the calculated frequencies may still differ from the experimental values.

## Acknowledgements

The authors thank the DFG-Center for Functional Nanostructures for funding.

- [1] C. Herrmann, M. Reiher, *Top. Curr. Chem.* **2007**, *268*, 85–132.
- [2] M. C. Thielges, M. D. Fayer, *Acc. Chem. Res.* **2012**, *45*, 1866–1874.
- [3] A. Remorino, R. M. Hochstrasser, *Acc. Chem. Res.* **2012**, *45*, 1896–1905.
- [4] T. A. Keiderling in *Circular Dichroism: Principles and Applications*, 2nd ed. (Eds.: N. Berova, K. Nakanishi, R. W. Woody), Wiley-VCH, New York, **2000**, pp. 621–666.
- [5] L. D. Barron, A. D. Buckingham, *Chem. Phys. Lett.* **2010**, *492*, 199–213.
- [6] J. Kapitán, V. Baumruk, P. Bour, *J. Am. Chem. Soc.* **2006**, *128*, 2438–2443.
- [7] V. Profant, V. Baumruk, X. Li, M. Safarik, P. Bour, *J. Phys. Chem. B* **2011**, *115*, 15079–15089.
- [8] H. Chi, W. R. W. Welch, J. Kubelka, T. A. Keiderling, *Biomacromolecules* **2013**, *14*, 3880–3891.
- [9] M. Cho, *Two-Dimensional Optical Spectroscopy*, CRC, Boca Raton, **2009**.
- [10] P. Hamm, M. Zanni, *Concepts and Methods of 2D Infrared Spectroscopy*, 1st ed Cambridge University Press, Cambridge, **2011**.
- [11] C. T. Middleton, P. Marek, P. Cao, C.-c. Chiu, S. Singh, A. M. Woys, J. J. de Pablo, D. P. Raleigh, M. T. Zanni, *Nat. Chem.* **2012**, *4*, 355–360.
- [12] J. Bredenbeck, J. Helbing, J. R. Kumita, G. A. Woolley, P. Hamm, *Proc. Natl. Acad. Sci. USA* **2005**, *102*, 2379–2384.
- [13] J. K. Chung, M. C. Thielges, M. D. Fayer, *J. Am. Chem. Soc.* **2012**, *134*, 12118–12124.
- [14] E. B. Wilson, J. C. Decius, P. C. Cross, *Molecular Vibrations: The Theory of Infrared and Raman Vibrational Spectra*, Dover, New York, **1980**.
- [15] C. R. Jacob, S. Luber, M. Reiher, *Chem. Eur. J.* **2009**, *15*, 13491–13508.
- [16] C. R. Jacob, *ChemPhysChem* **2011**, *12*, 3291–3306.
- [17] S. Luber, *J. Phys. Chem. A* **2013**, *117*, 2760–2770.
- [18] S. Luber, M. Reiher, *J. Phys. Chem. B* **2010**, *114*, 1057–1063.
- [19] M. Reiher, J. Neugebauer, *J. Chem. Phys.* **2003**, *118*, 1634–1641.
- [20] C. Herrmann, J. Neugebauer, M. Reiher, *New J. Chem.* **2007**, *31*, 818–831.
- [21] K. Kiewisch, J. Neugebauer, M. Reiher, *J. Chem. Phys.* **2008**, *129*, 204103.
- [22] S. Luber, J. Neugebauer, M. Reiher, *J. Chem. Phys.* **2009**, *130*, 064105.
- [23] P. Bouř, J. Sopková, L. Bednářová, P. Maloň, T. A. Keiderling, *J. Comput. Chem.* **1997**, *18*, 646–659.
- [24] N. S. Bieler, M. P. Haag, C. R. Jacob, M. Reiher, *J. Chem. Theory Comput.* **2011**, *7*, 1867–1881.
- [25] S. Yamamoto, X. Li, K. Ruud, P. Bour, *J. Chem. Theory Comput.* **2012**, *8*, 977–985.
- [26] B. Temelso, G. C. Shields, *J. Chem. Theory Comput.* **2011**, *7*, 2804–2817.
- [27] T. Fornaro, M. Biczysko, S. Monti, V. Barone, *Phys. Chem. Chem. Phys.* **2014**, *6*, 10112–10128.

- [28] See for example: N. C. Polfer, J. Oomens, S. Suhai, B. Paizs, *J. Am. Chem. Soc.* **2007**, *129*, 5887–5897.
- [29] See for example: E. G. Buchanan, W. H. James, S. H. Choi, L. Guo, S. H. Gellman, C. W. Müller, T. S. Zwier, *J. Chem. Phys.* **2012**, *137*, 094301.
- [30] See for example: F. Schinle, P. E. Crider, M. Vonderach, P. Weis, O. Hampe, M. M. Kappes, *Phys. Chem. Chem. Phys.* **2013**, *15*, 6640–6650.
- [31] F. Schinle, C. R. Jacob, A. B. Wolk, J.-F. Greisch, M. Vonderach, P. Weis, O. Hampe, M. A. Johnson, M. M. Kappes, *J. Phys. Chem. A* **2014**, DOI: 10.1021/jp501772d.
- [32] V. Barone, M. Biczysko, J. Bloino, *Phys. Chem. Chem. Phys.* **2014**, *16*, 1759–1787.
- [33] M. Thomas, M. Brehm, R. Fligg, P. Vöhringer, B. Kirchner, *Phys. Chem. Chem. Phys.* **2013**, *15*, 6608–6622.
- [34] R. Ramírez, T. López-Ciudad, P. Kumar, P. D. Marx, *J. Chem. Phys.* **2004**, *121*, 3973.
- [35] R. D. Amos, N. C. Handy, W. H. Green, D. Jayatilaka, A. Willetts, P. Palmieri, *J. Chem. Phys.* **1991**, *95*, 8323–8336.
- [36] K. M. Kuhler, D. G. Truhlar, A. D. Isaacson, *J. Chem. Phys.* **1996**, *104*, 4664–4671.
- [37] V. Barone, *J. Chem. Phys.* **2005**, *122*, 014108.
- [38] T. K. Roy, R. B. Gerber, *Phys. Chem. Chem. Phys.* **2013**, *15*, 9468–9492.
- [39] J. K. G. Watson, *Mol. Phys.* **1968**, *15*, 479–490.
- [40] N. J. Wright, R. B. Gerber, *J. Chem. Phys.* **2000**, *112*, 2598–2604.
- [41] A. G. Császár, N. C. Handy, *J. Chem. Phys.* **1995**, *102*, 3962–3967.
- [42] S. N. Yurchenko, W. Thiel, P. Jensen, *J. Mol. Spectrosc.* **2007**, *245*, 126–140.
- [43] J. Pesonen, K. O. E. Henriksson, J. R. López-Blanco, P. Chacón, *J. Math. Chem.* **2012**, *50*, 1521–1549.
- [44] J. O. Jung, R. B. Gerber, *J. Chem. Phys.* **1996**, *105*, 10332–10348.
- [45] S. Carter, S. J. Culik, J. M. Bowman, *J. Chem. Phys.* **1997**, *107*, 10458–10469.
- [46] S. Carter, H. M. Shnyder, J. M. Bowman, *J. Chem. Phys.* **1999**, *110*, 8417–8423.
- [47] G. Rauhut, *J. Chem. Phys.* **2004**, *121*, 9313–9322.
- [48] L. Pele, R. B. Gerber, *J. Chem. Phys.* **2008**, *128*, 165105.
- [49] D. M. Benoit, *J. Chem. Phys.* **2004**, *120*, 562.
- [50] V. Barone, M. Biczysko, J. Bloino, M. Borkowska-Panek, I. Carnimeo, P. Panek, *Int. J. Quantum Chem.* **2012**, *112*, 2185–2200.
- [51] C. R. Jacob, M. Reiher, *J. Chem. Phys.* **2009**, *130*, 084106.
- [52] C. R. Jacob, S. Lubber, M. Reiher, *J. Phys. Chem. B* **2009**, *113*, 6558–6573.
- [53] V. Liégeois, C. R. Jacob, B. Champagne, M. Reiher, *J. Phys. Chem. A* **2010**, *114*, 7198–7212.
- [54] T. Weymuth, C. R. Jacob, M. Reiher, *J. Phys. Chem. B* **2010**, *114*, 10649–10660.
- [55] S. Mukamel, *Principles of Nonlinear Optical Spectroscopy*, Oxford University Press, New York, **1999**.
- [56] G. Firanescu, R. Signorell, *J. Phys. Chem. B* **2009**, *113*, 6366–6377.
- [57] W. Zhuang, T. Hayashi, S. Mukamel, *Angew. Chem.* **2009**, *121*, 3804–3838; *Angew. Chem. Int. Ed.* **2009**, *48*, 3750–3781.
- [58] J. Jeon, S. Yang, J.-H. Choi, M. Cho, *Acc. Chem. Res.* **2009**, *42*, 1280–1289.
- [59] P. Hamm, M. Lim, R. M. Hochstrasser, *J. Phys. Chem. B* **1998**, *102*, 6123–6138.
- [60] S. Krimm, Y. Abe, *Proc. Natl. Acad. Sci. USA* **1972**, *69*, 2788–2792.
- [61] H. Torii, *J. Phys. Chem. A* **2004**, *108*, 7272–7280.
- [62] T. la Cour Jansen, J. Knoester, *J. Chem. Phys.* **2006**, *124*, 044502.
- [63] S. Roy, J. Lessing, G. Meisl, Z. Ganim, A. Tokmakoff, J. Knoester, T. L. C. Jansen, *J. Chem. Phys.* **2011**, *135*, 234507.
- [64] S. M. Gruenbaum, C. J. Tainter, L. Shi, Y. Ni, J. L. Skinner, *J. Chem. Theory Comput.* **2013**, *9*, 3109–3117.
- [65] G. Rauhut, *J. Chem. Phys.* **2007**, *127*, 184109.
- [66] Y. Wang, J. M. Bowman, *Chem. Phys. Lett.* **2010**, *491*, 1–10.
- [67] J. S. Mancini, J. M. Bowman, *J. Chem. Phys.* **2013**, *139*, 164115.
- [68] Y. Wang, J. M. Bowman, *J. Chem. Phys.* **2012**, *136*, 144113.
- [69] T. C. Thompson, D. G. Truhlar, *J. Chem. Phys.* **1982**, *77*, 3031–3035.
- [70] K. Yagi, M. Keceli, S. Hirata, *J. Chem. Phys.* **2012**, *137*, 204118.
- [71] B. Thomsen, K. Yagi, O. Christiansen, *J. Chem. Phys.* **2014**, *140*, 154102.
- [72] J. M. Bowman, *Acc. Chem. Res.* **1986**, *19*, 202–208.
- [73] I. P. Hamilton, J. C. Light, *J. Chem. Phys.* **1986**, *84*, 306–317.
- [74] W. Yang, A. C. Peet, *Chem. Phys. Lett.* **1988**, *153*, 98–104.
- [75] O. Christiansen, *Phys. Chem. Chem. Phys.* **2007**, *9*, 2942–2953.
- [76] O. Christiansen, *Phys. Chem. Chem. Phys.* **2012**, *14*, 6672–6687.
- [77] J. M. Bowman, K. Christoffel, F. Tobin, *J. Phys. Chem.* **1979**, *83*, 905–912.
- [78] M. Neff, G. Rauhut, *J. Chem. Phys.* **2009**, *131*, 124129.
- [79] P. Seidler, O. Christiansen, *J. Chem. Phys.* **2007**, *126*, 204101.
- [80] Y. Watanabe, S. Maeda, K. Ohno, *J. Chem. Phys.* **2008**, *129*, 074315.
- [81] D. Bégué, I. Baraille, P. A. Garrain, A. Dargelos, T. Tassaing, *J. Chem. Phys.* **2010**, *133*, 034102.
- [82] Y. Wang, X. Huang, B. C. Shepler, B. J. Braams, J. M. Bowman, *J. Chem. Phys.* **2011**, *134*, 094509.
- [83] J. H. Choi, S. Ham, M. Cho, *J. Phys. Chem. B* **2003**, *107*, 9132–9138.
- [84] R. D. Gorbunov, D. S. Kosov, G. Stock, *J. Chem. Phys.* **2005**, *122*, 224904.
- [85] C. R. Jacob, S. M. Beyhan, R. E. Bulo, A. S. P. Gomes, A. W. Götz, K. Kiewisch, J. Sikkema, L. Visscher, *J. Comput. Chem.* **2011**, *32*, 2328–2338.
- [86] T. E. Oliphant, *Comput. Sci. Eng.* **2007**, *9*, 10–20.
- [87] R. Ahlrichs, et al., Turbomole, URL: <http://www.turbomole.com>.
- [88] R. Ahlrichs, M. Bär, M. Häser, H. Horn, C. Kölmel, *Chem. Phys. Lett.* **1989**, *162*, 165–169.
- [89] A. D. Becke, *Phys. Rev. A* **1988**, *38*, 3098–3100.
- [90] J. P. Perdew, *Phys. Rev. B* **1986**, *33*, 8822–8824.
- [91] A. Schäfer, C. Huber, R. Ahlrichs, *J. Chem. Phys.* **1994**, *100*, 5829–5835.
- [92] K. Eichkorn, O. Treutler, H. Öhm, M. Häser, R. Ahlrichs, *Chem. Phys. Lett.* **1995**, *240*, 283–289.
- [93] K. Eichkorn, F. Weigend, O. Treutler, R. Ahlrichs, *Theor. Chem. Acc.* **1997**, *97*, 119–124.
- [94] J. Neugebauer, M. Reiher, C. Kind, B. A. Hess, *J. Comput. Chem.* **2002**, *23*, 895–910.
- [95] T. Weymuth, M. P. Haag, K. Kiewisch, S. Lubber, S. Schenk, C. R. Jacob, C. Herrmann, J. Neugebauer, M. Reiher, *J. Comput. Chem.* **2012**, *33*, 2186–2198.
- [96] E. Jones, T. Oliphant, P. Peterson, et al., Numpy | A python library for numerical computations, URL: <http://www.scipy.org/NumPy>.

Received: April 17, 2014

Published online on July 30, 2014